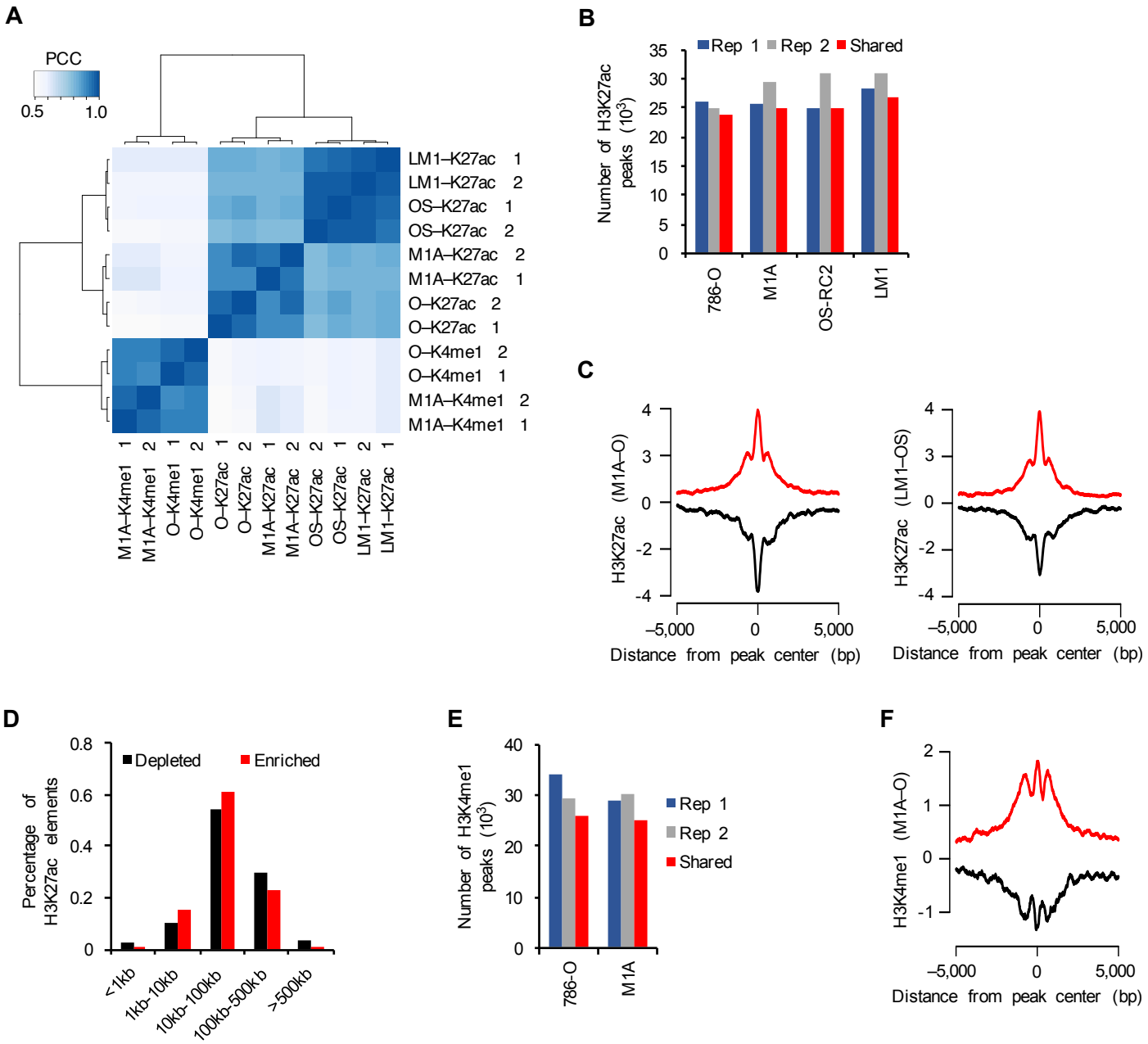

Supplementary Figure 1. Enhancer mapping in metastatic RCC cells. A, Genome wide correlation of H3K27ac and H3K4me1 ChIP-seq signal across different samples and replicates. PCC, Pearson's correlation coefficient. **B,** Number of H3K27ac peaks relative to input in different samples and replicates. **C,** Average difference in H3K27ac signal between the metastatic and non-metastatic cells normalized to corresponding input sample at H3K27ac-enriched (red) and H3K27ac-depleted (black) genomic regions in both experimental systems. **D,** Distances of H3K27ac-enriched and H3K27ac-depleted regions from known transcription start sites. **E,** Number of H3K4me1 peaks relative to input in replicates of 786-O and M1A cells. **F,** Average difference in H3K4me1 signal between the metastatic and non-metastatic cells normalized to corresponding input sample at H3K27ac-enriched (red) and H3K27ac-depleted (black) genomic regions in the 786 system.

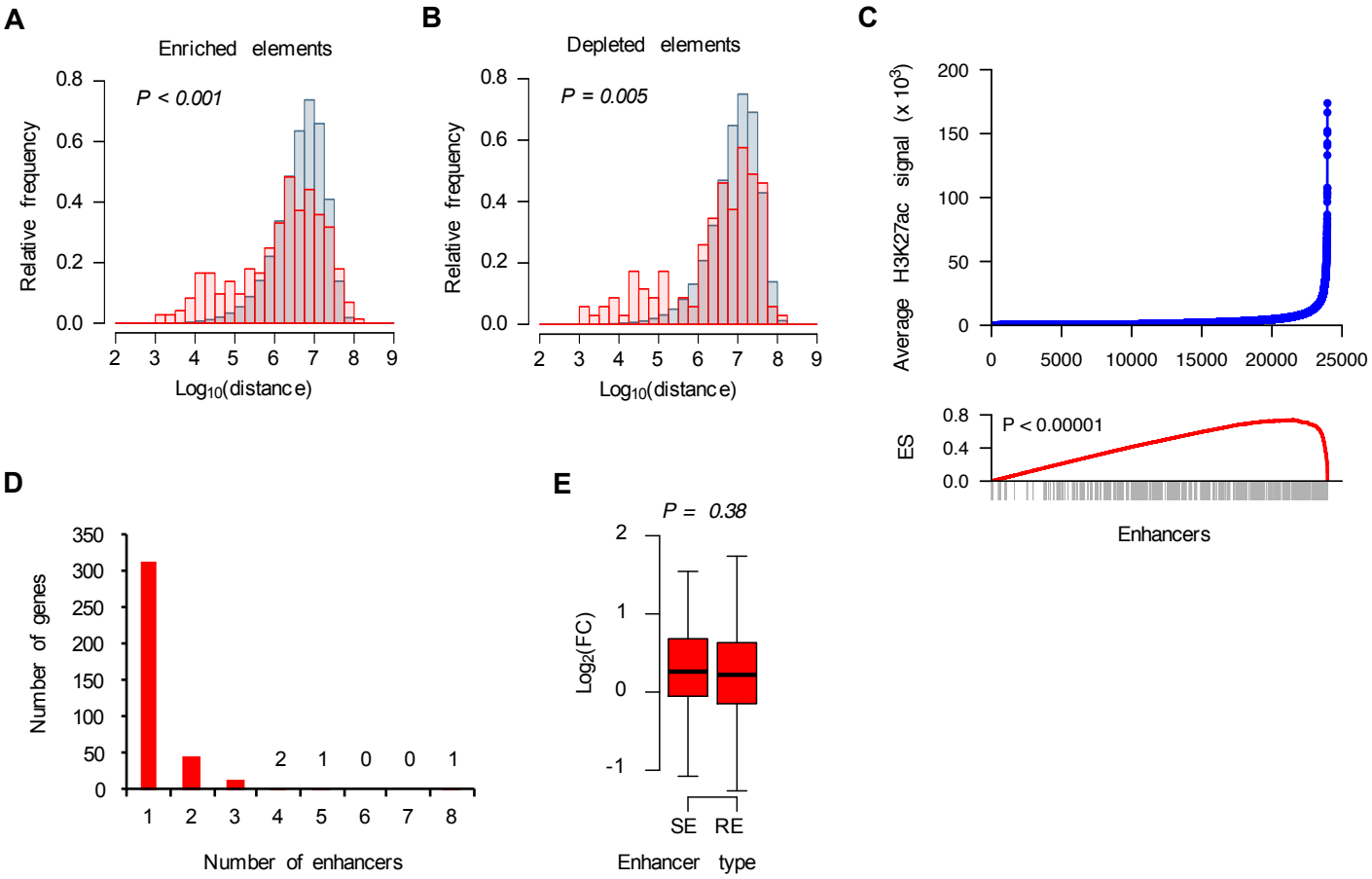

Supplementary Figure 2. Metastasis-associated enhancers (MAEs) are preferentially located within super enhancers. **A,** Distances between the 314 H3K27ac-enriched genomic elements within each chromosome. Observed data in red, simulated data in blue. Empirical P-values calculated using the Wilcoxon rank-sum test with 10,000 permutations. **B,** Distances between 161 depleted genomic elements within each chromosome. Observed data in red, simulated data in blue. Empirical P-values calculated using the Wilcoxon rank-sum test with 10,000 permutations. **C,** Top, Average H3K27ac signal across all samples and enhancer regions. Bottom, gene set enrichment analysis (GSEA) of the enriched and depleted H3K27ac regions (grey bars) relative to the average H3K27ac signal shown in the top panel. Empirical P-value calculated using 10,000 permutations. **D,** Number of genes with different numbers of associated MAEs. **E,** Relative mRNA expression of transcripts with associated super enhancers (SE) or regular enhancers (RE) containing altered H3K27ac regions. Data from two RNA-seq experiments for both 786 and OS systems combined, whiskers 1.5 x interquartile range. Wilcoxon rank-sum test.

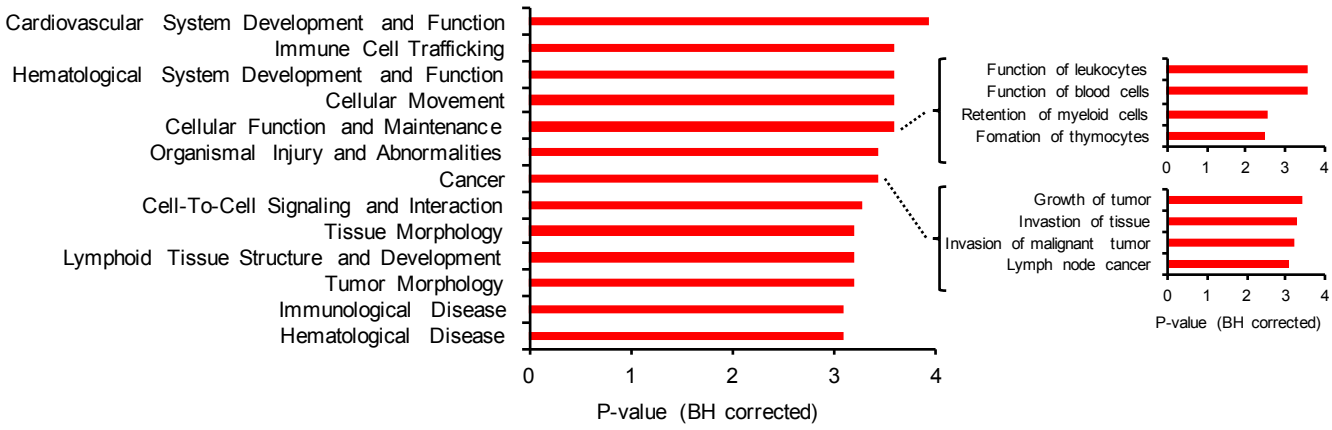

Supplementary Figure 3. Ingenuity Pathway Analysis (IPA) on the H3K27ac-enriched MAE-associated gene set. B-H multiple testing corrected P-value of <0.001 was considered significant.

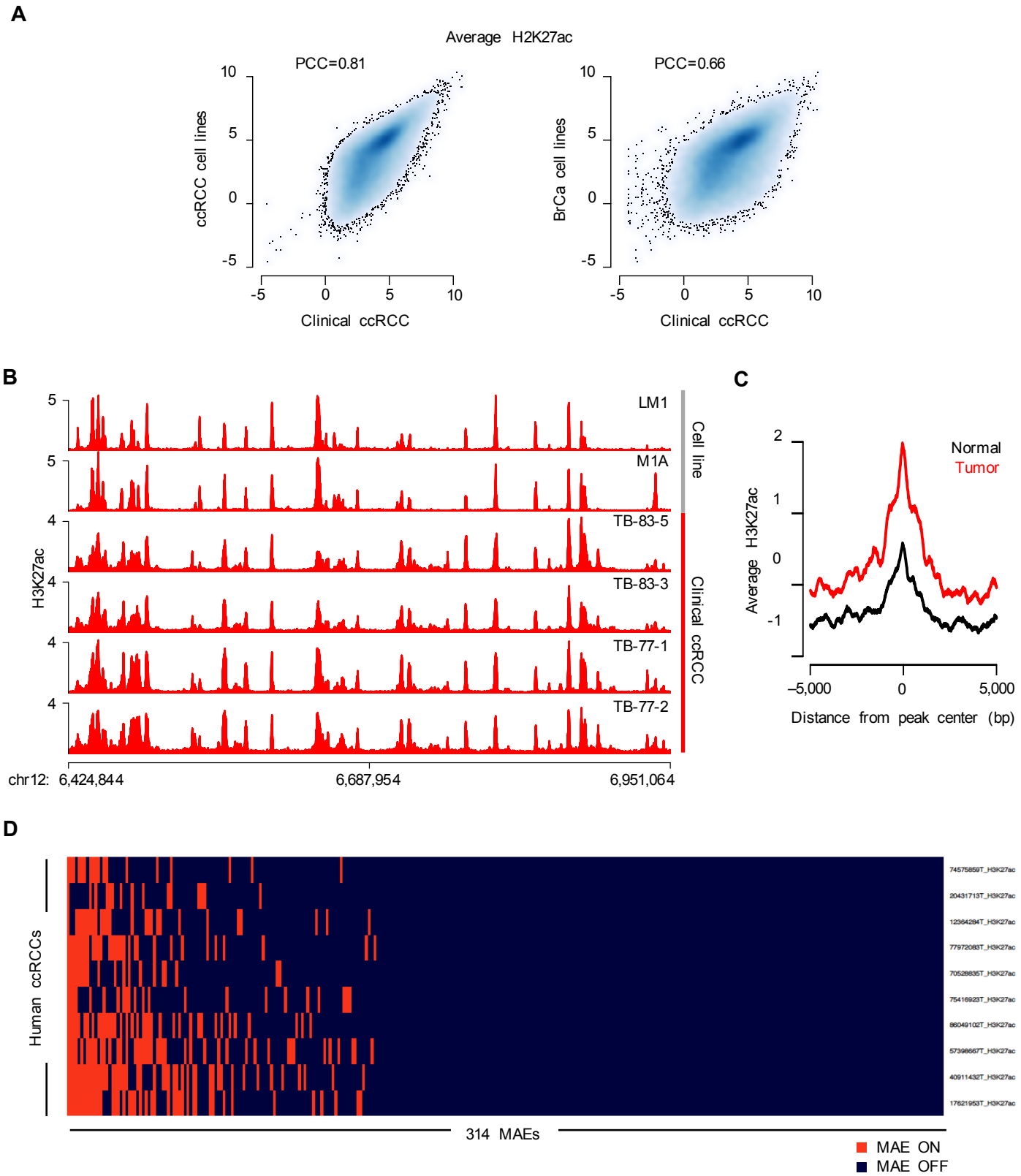

Supplementary Figure 4. Metastasis-associated enhancers in human ccRCC samples. A, Average ChIP-seq signal (log2) in cell lines and clinical samples across 38,625 H3K27ac-enriched regions. PCC, Pearson's correlation coefficient. **B,** Examples of H3K27ac-enriched genomic regions in cell lines and ccRCC clinical samples. **C,** Average H3K27ac signal in normal kidney (black) and ccRCC samples (red) normalized to corresponding input samples at H3K27ac-enriched MAEs. **D,** MAE activation patterns in human ccRCC samples compared to matched normal tissue.

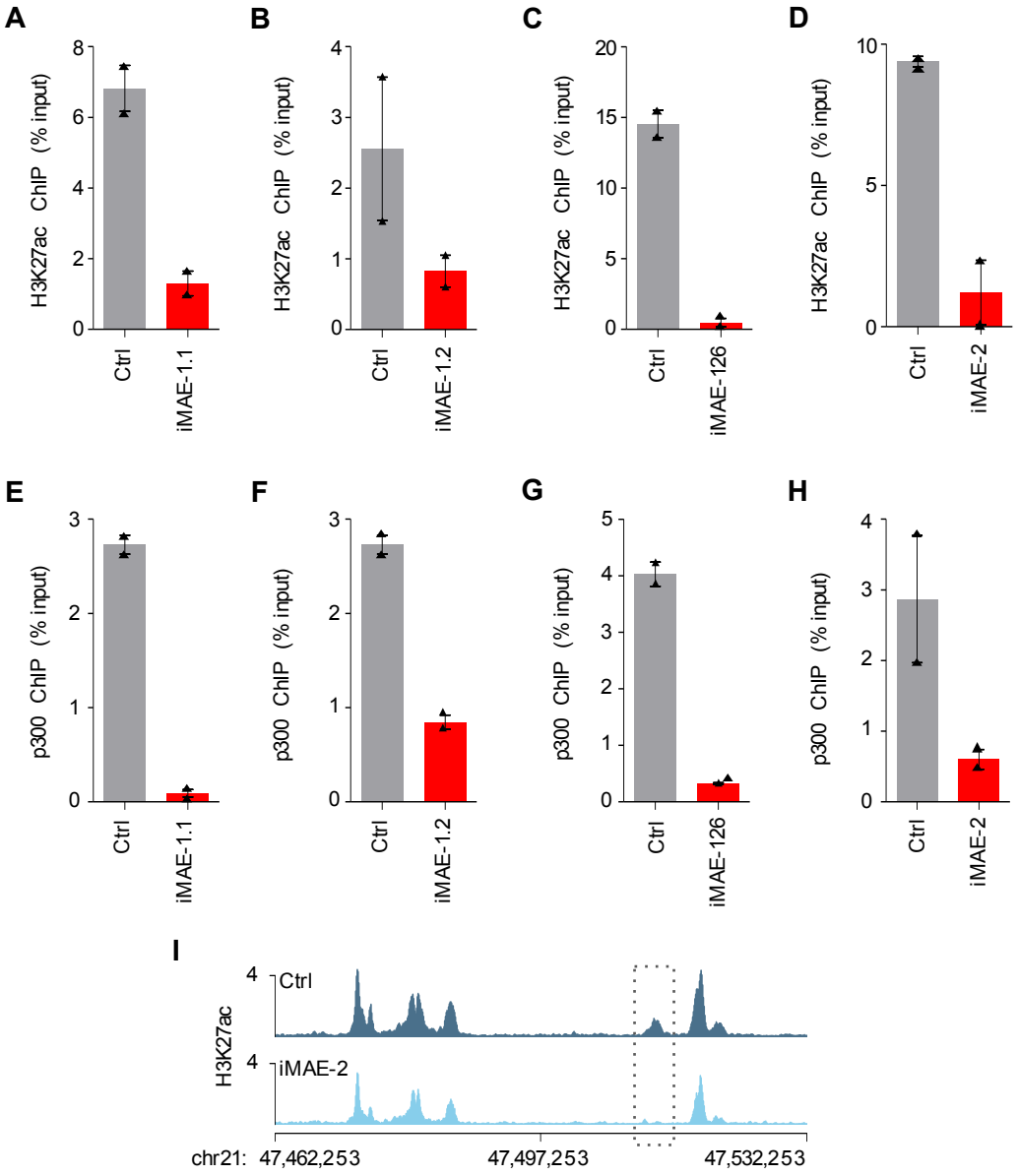

Supplementary Figure 5. Enhancer targeting by CRISPRi. A-D, H3K27ac ChIP-qPCR validation of CRISPRi-mediated enhancer targeting. Mean of two experiments. Error bars S.E.M. **E-H,** p300 ChIP-qPCR validation of CRISPRi-mediated enhancer targeting Mean of two experiments. Error bars S.E.M. **I,** H3K27ac ChIP-seq signal showing the effects of CRISPRi-mediated targeting of MAE-2. The intended target region highlighted by the grey box.

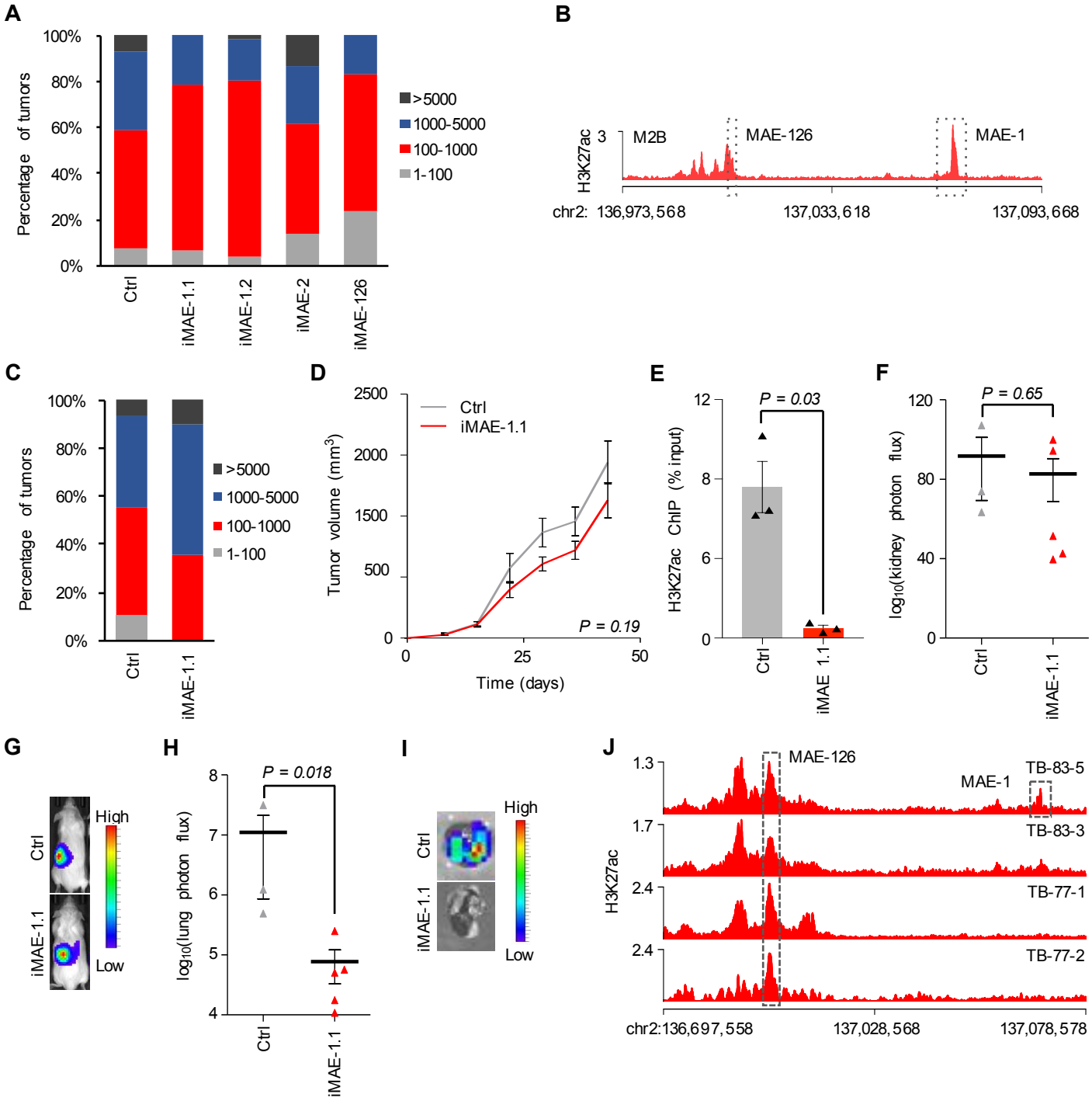

Supplementary Figure 6. Phenotypic effects of CRISPRi-mediated enhancer targeting. A, Size distribution of lung metastases for the experiment shown in Figure 3A. N=3 for Ctrl, N=4 for iMAE-1.1, N=3 for iMAE-1.2, N=3 for iMAE-2, N=5 for iMAE-126**. B,** H3K27ac ChIP-seq signal in the MAE-1/MAE-126 locus on chromosome 2 in M2B cells. **C,** Size distribution of lung metastases for the experiment shown in Figure 3E. N=3 for both groups. **D,** Subcutaneous growth of M1A cells with CRISPRi-mediated targeting of MAE-1. N=8 in both groups. Whiskers represent S.D. Two-sided Student's T-test. **E,** H3K27ac ChIP-qPCR on subcutaneous tumors from the experiment shown in panel D. Mean data from three tumors, whiskers represent S.E.M. Two-sided Student's T-test. **F,** Renal growth of M1A cells with CRISPRi-mediated targeting of MAE-1. N=3 for Ctrl, N=5 for iMAE-1.1. Whiskers represent S.E.M. P-value calculated by one-tailed Wilcoxon rank-sum test. **G,** Representative bioluminescence images for the experiment shown in F. **H,** *Ex vivo* lung photon flux for the experiment shown in F nine weeks after tumor induction. Whiskers represent S.E.M. P-value calculated by one-tailed Wilcoxon rank-sum test. **I,** Representative bioluminescence images for the data shown in H. **J,** H3K27ac ChIP-seq signal in the MAE-1/MAE-126 locus on chromosome 2 in ccRCC clinical samples.

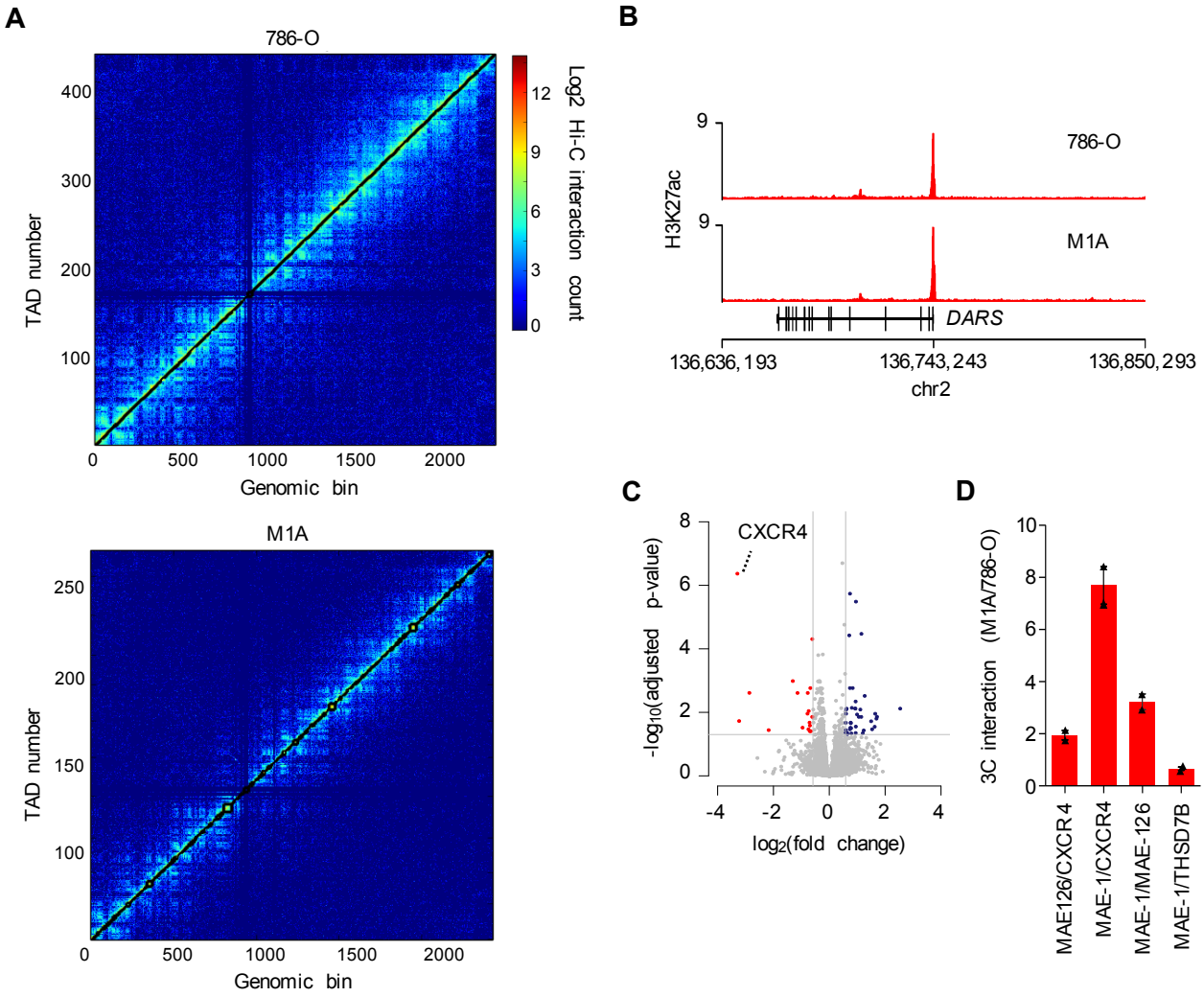

Supplementary Figure 7. Chromatin state at the MAE-1/MAE-126 locus. A, Global HiC profile of chromosome 2 in the 786-O and M1A cells. 40kb resolution. **B,** H3K27ac ChIP-seq tracks showing the *DARS* locus in ccRCC cells. **C,** Global transcriptomic effects of CRISPRi-mediated MAE-1/MAE-126 targeting. **D,** Chromosome conformation capture 3C analysis of the MAE-1/MAE-126 locus. Mean of two experiments. Error bars S.E.M.

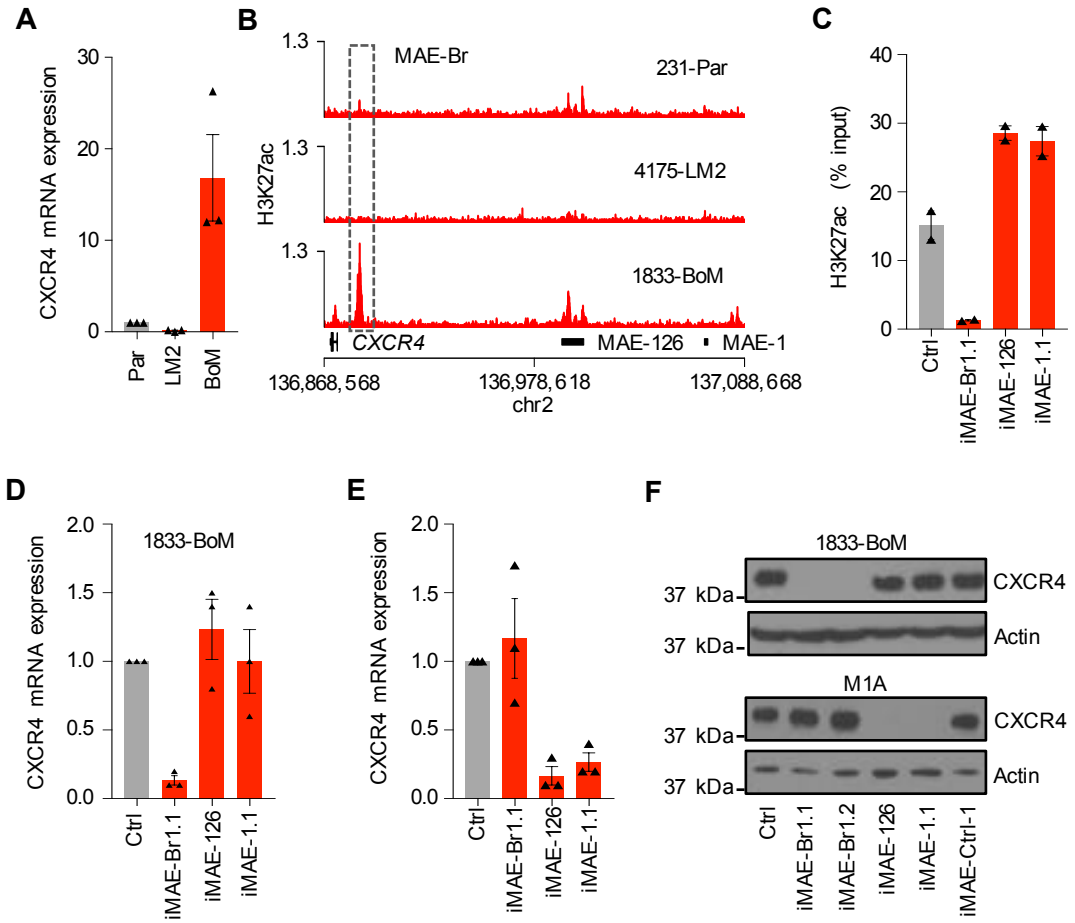

Supplementary Figure 8. CRISPRi-mediated enhancer targeting in metastatic triple negative breast cancer cells. A, *CXCR4* mRNA expression as measured by qRT-PCR in the MDA-MB-231 metastasis model of triple negative breast cancer. Mean of three experiments. Error bars S.E.M. **B,** H3K27ac ChIP-seq tracks showing the CXCR4/MAE-126/MAE-1 locus in the MDA-231 breast cancer models. MAE-Br highlighted by the grey box. **C,** H3K27ac ChIP-qPCR for the MAE-Br locus in 1833-BoM cells with CRISPRi targeting of MAE-Br, MAE-1 and MAE-126. Mean of two experiments. Error bars S.E.M. **D-E,** *CXCR4* mRNA expression in 1833-BoM (D) and M1A (E) cells as measured by qRT-PCR. Mean of three experiments. Error bars S.E.M. **F,** CXCR4 protein expression as measured by immunoblotting. iMAE-Ctrl-1 targets a region between MAE-Br and MAE-126 showing no H3K27ac enrichment in either 1833-BoM or M1A cells. A representative experiment of three is shown.

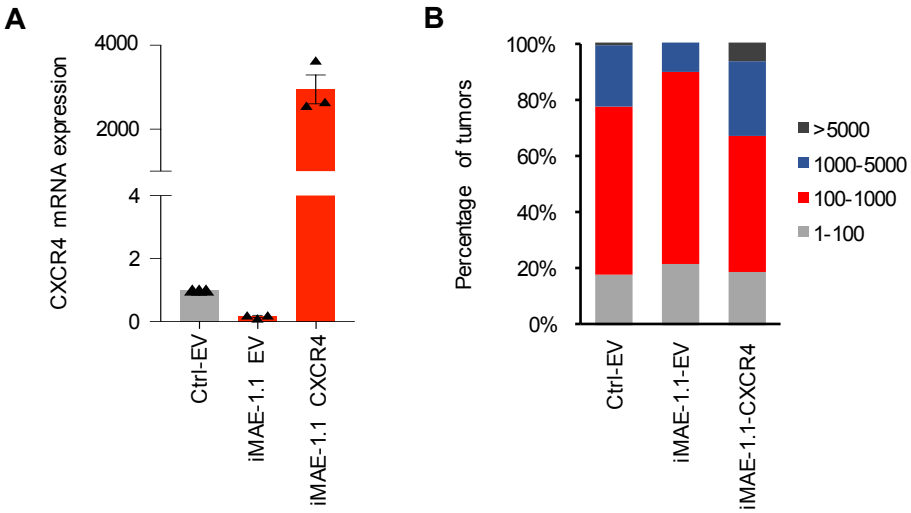

Supplementary Figure 9. CXCR4 as a functional effector of the MAE-1/MAE-126 locus. **A,** *CXCR4* mRNA expression as measured by qRT-PCR in M1A cells expressing the indicated constructs. Mean of three experiments. Error bars S.E.M. **B,** Size distribution of lung metastases for the experiment shown in Figure 5A. For each group, N=3.

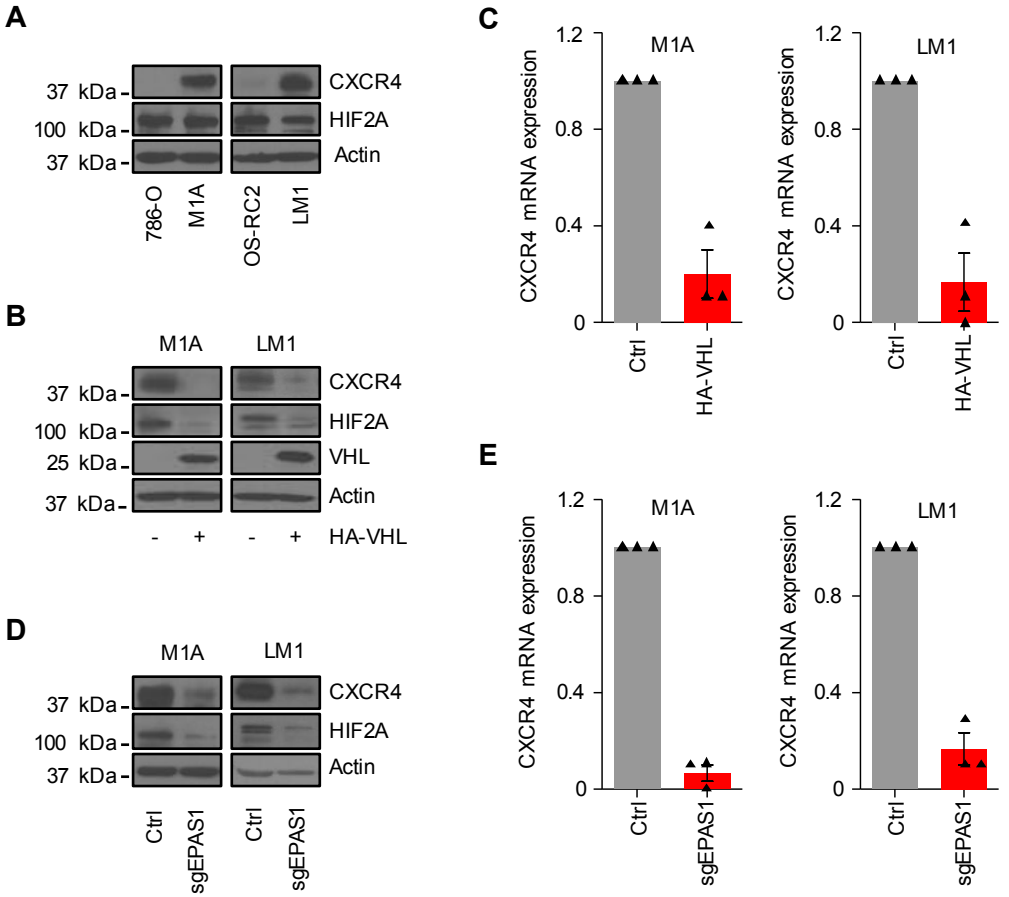

Supplementary Figure 10. HIF2A regulates CXCR4 expression. A, CXCR4 and HIF2A protein expression in parental and metastatic ccRCC cells as measured by immunoblotting. **B-C,** CXCR4 protein (B) and mRNA (C) expression in metastatic ccRCC cells in response to VHL re-introduction. **D-E,** CXCR4 protein (D) and mRNA (E) expression in metastatic ccRCC cells in response to HIF2A CRISPR/Cas9 knock-down. Immunoblots, a representative experiment of three is shown. qRT-PCR, mean of three experiments. Error bars S.E.M.

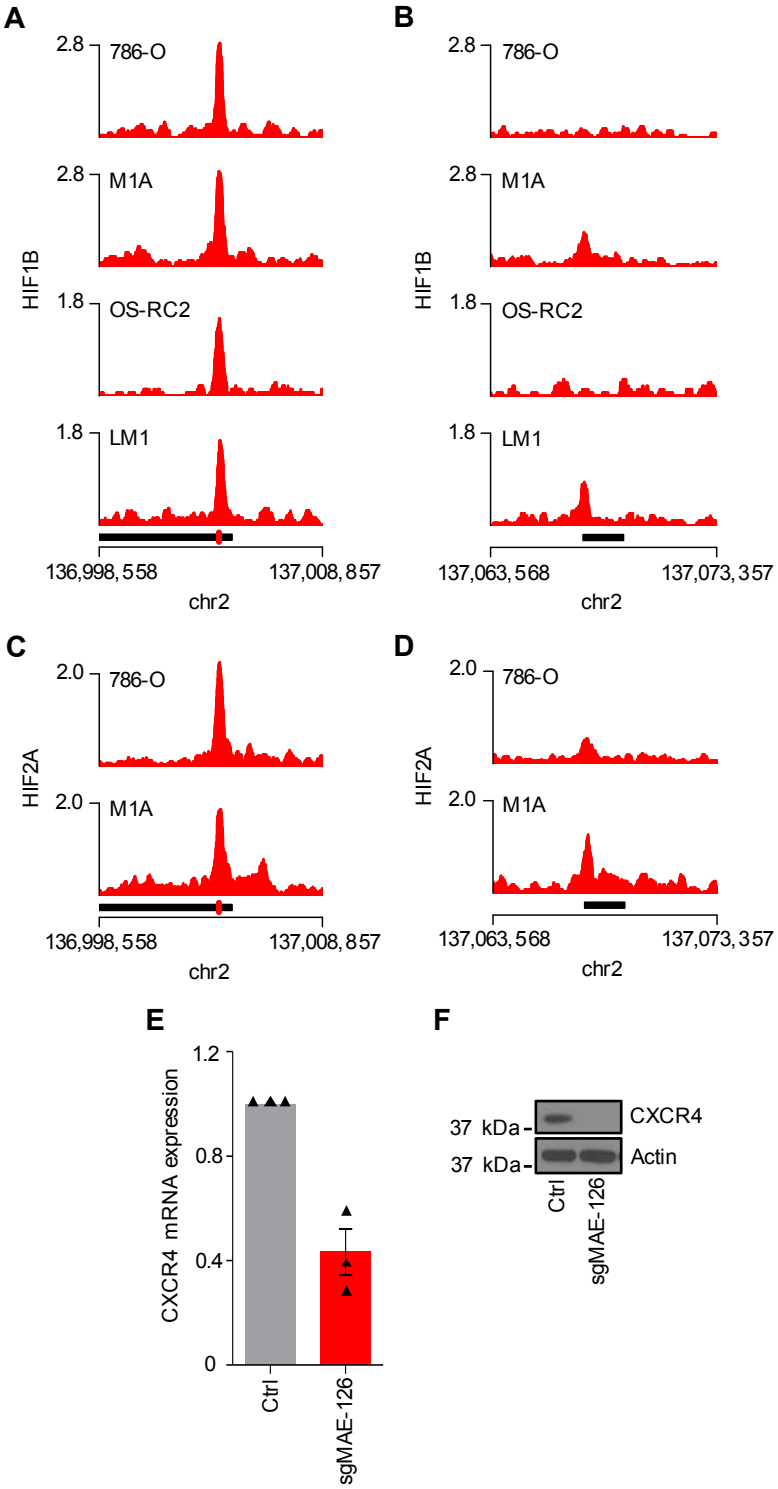

Supplementary Figure 11. HIF1B/HIF2A binding at the MAE-126 locus. A, HIF1B ChIP-seq signal in the MAE-126 locus. Black bar indicates MAE-126, the red line shows the location of a HIF binding motif. **B,** HIF1B ChIP-seq signal in the MAE-1 locus, black bar indicates MAE-1. **C,** HIF2A ChIP-seq signal in the MAE-126 locus. Black bar indicates MAE-126, the red line shows the location of a HIF binding motif. **D,** HIF2A ChIP-seq signal in the MAE-1 locus, black bar indicates MAE-1. **E,** *CXCR4* mRNA expression in M1A cells as measured by qRT-PCR. Mean of three experiments. Error bars S.E.M. **F,** CXCR4 protein expression in M1A cells as measured by immunoblotting. A representative experiment of three is shown.

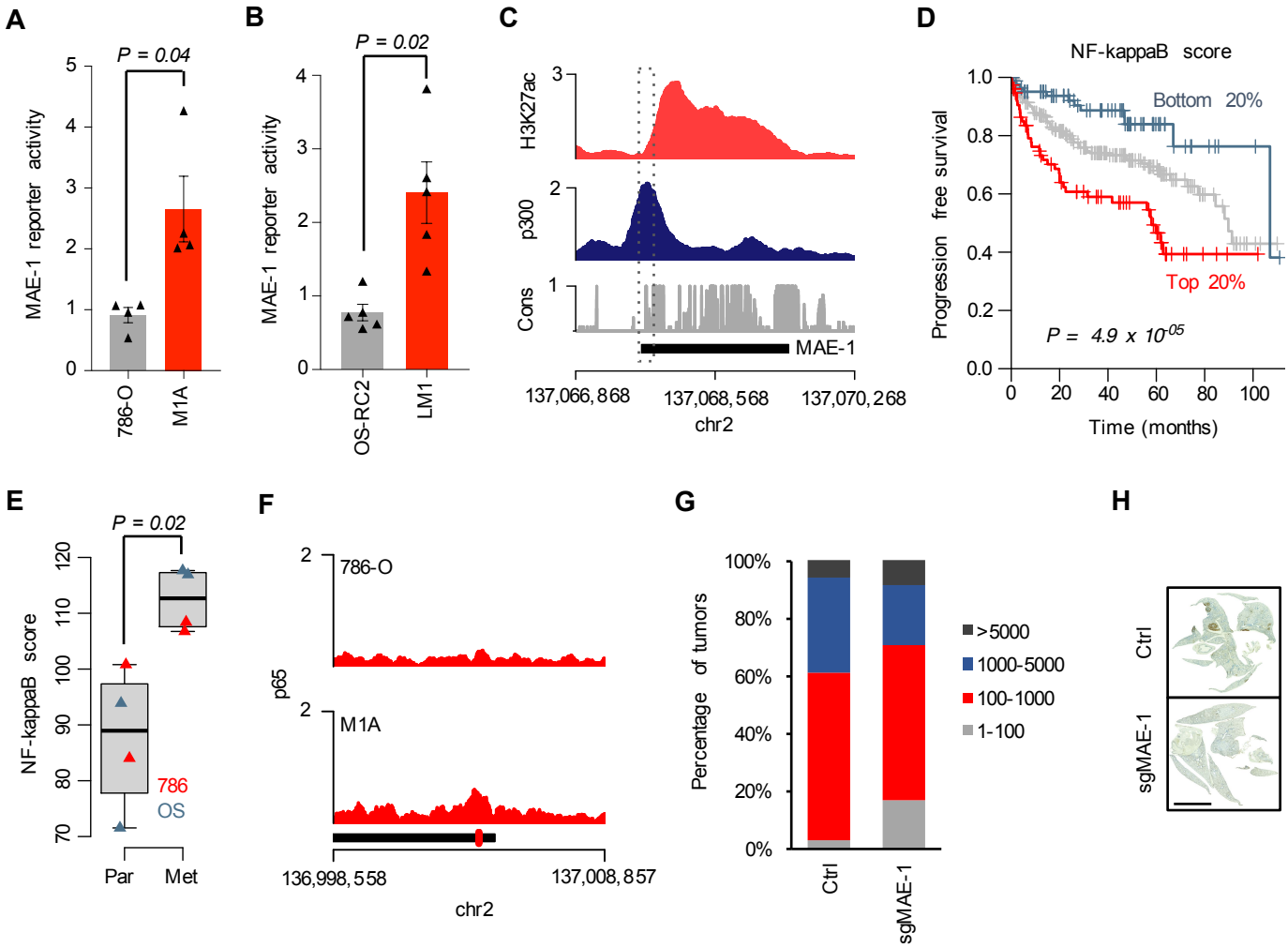

Supplementary Figure 12. MAE-1 activation associated with NF-kappaB activity in metastatic ccRCC clones. A-B, Transient reporter assays showing enhancer activity of the MAE-1 sequence. Mean of four (786) and five (OS) experiments. Error bars S.E.M. Two-sided Student's t-test. **C,** H3K27ac and p300 ChIP-seq signal in relation to evolutionary conservation of the MAE-1 locus. Conservation score by PhastCons. Grey box highlights a conserved p65/RELA motif. **D,** Progression free survival in the TCGA ccRCC cohort, patients categorized based on the sum of Z-scores of NF-kappaB signature mRNAs, top 20% in red, bottom 20% in blue, middle 60% in grey. P-value derived from a Cox proportional hazards model in which sum of Z-scores is used as a continuous variable. N=400. **E,** NF-kappaB activation score determined as the sum of Z-scores of NF-kappaB signature mRNAs. Two-sided Student's t-test. **F,** p65 ChIP-seq signal in the MAE-126 locus. Black bar indicates MAE-126. Red line indicates the HIF2A binding site. **G,** Size distribution of lung metastases for the experiment shown in Figure 6H. N=3 for both groups. **H,** Representative human vimentin immunohistochemistry of mouse lungs quantified in panels G. Scale bar 5mm.

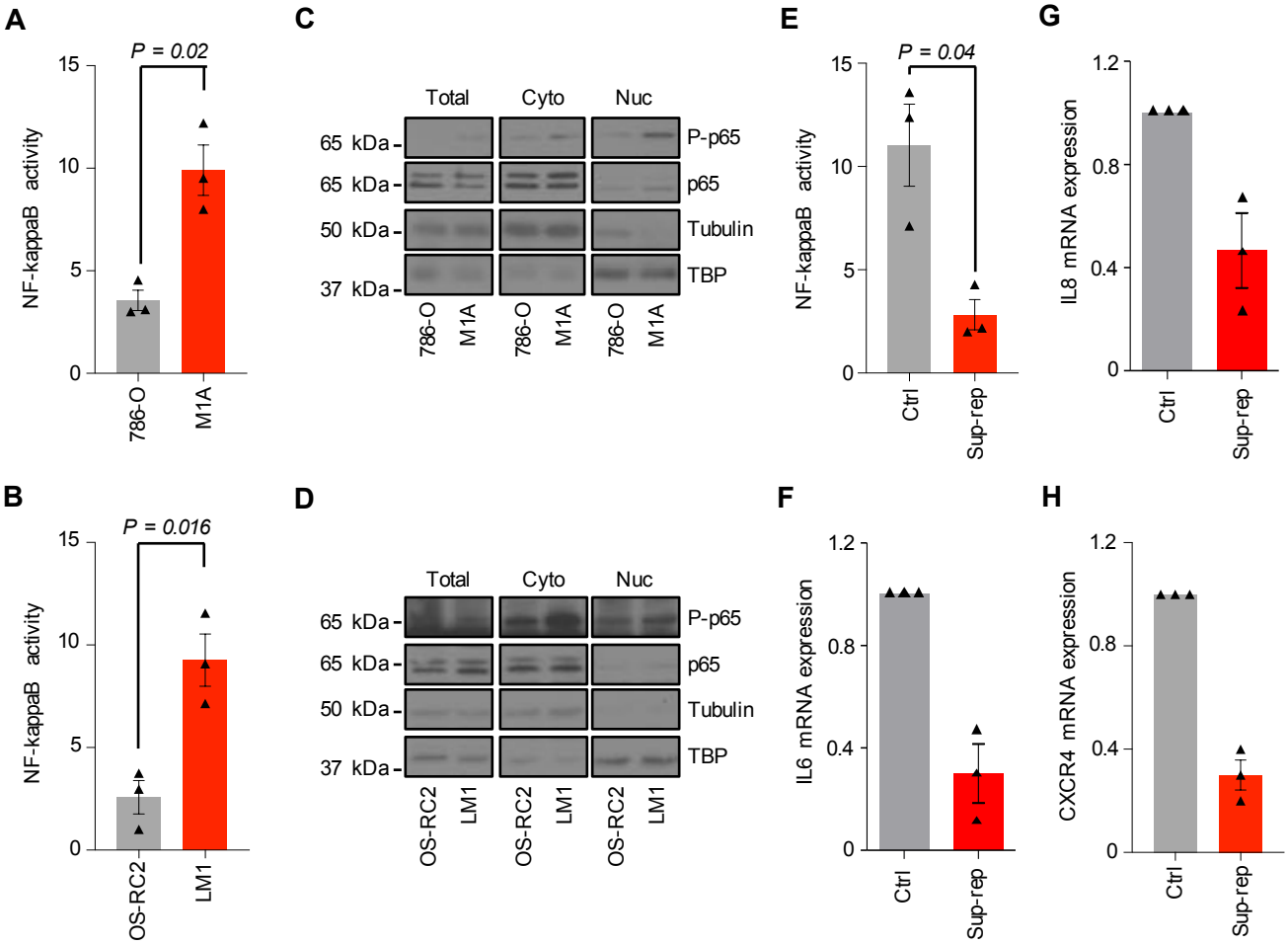

Supplementary Figure 13. NF-kappaB activity in metastatic ccRCC cells. A-B, Transient NF-kappaB reporter assay in parental and metastatic ccRCC cells. Mean of three experiments. Error bars S.E.M. Two-sided Student's t-test. **C-D,** NF-kappaB activation in metastatic ccRCC cells by immunoblotting. A representative experiment of three is shown. **E,** Transient NF-kappaB reporter assay in M1A cells expressing the NF-kappaB super repressor mutant IKBA. Mean of three experiments. Error bars S.E.M. Two-sided Student's t-test. **F-H,** Expression of *IL6*, *IL8* and *CXCR4* mRNA in M1A cells expressing the NF-kappaB super repressor. Mean of three experiments. Error bars S.E.M.

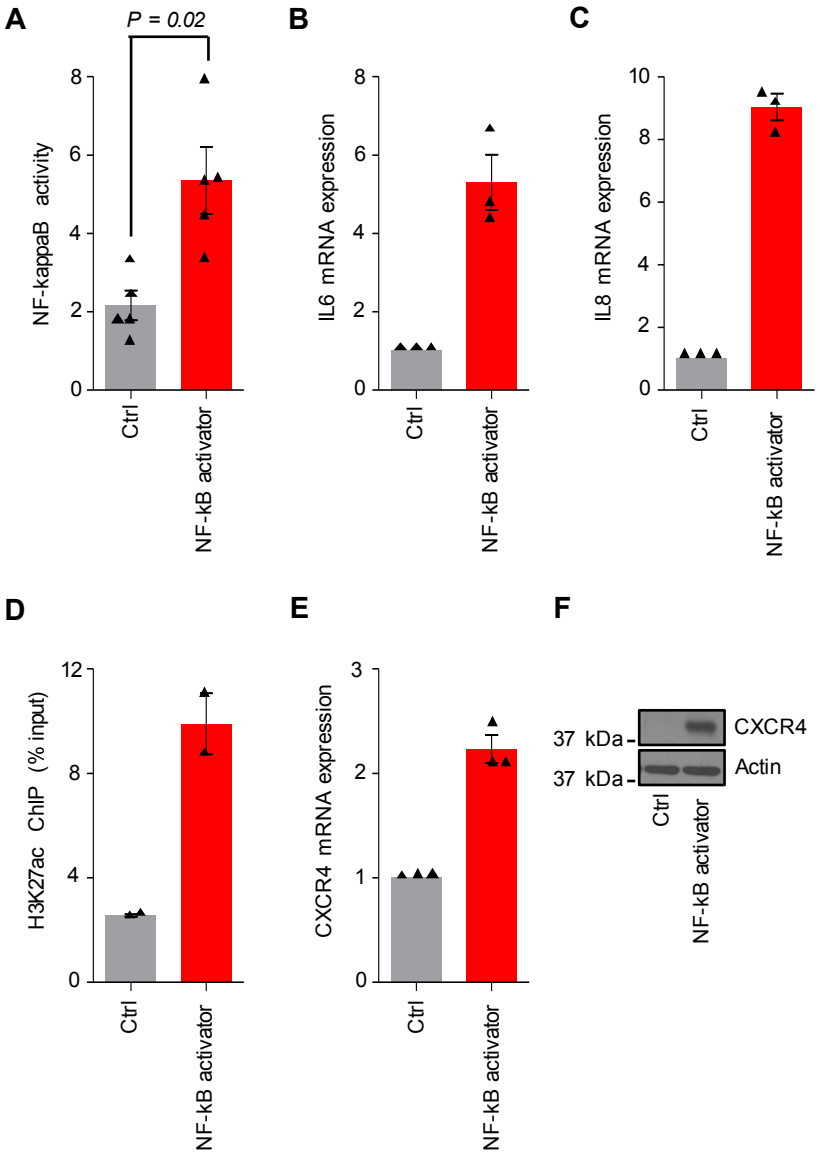

Supplementary Figure 14. NF-kappaB super activation in non-metastatic ccRCC cells. A, Transient NF-kappaB reporter assay in 786-O cells expressing the NF-kappaB activator mutant IKK2. Mean of five independent experiments. Error bars S.E.M. Two-sided Student's t-test. **B-C,** Expression of *IL6* and *IL8* mRNA in 786-O cells expressing the NF-kappaB activator mutant IKK2. Mean of three experiments. Error bars S.E.M. **D,** H3K27ac ChIP-qPCR in the MAE-1 locus of 786-O cells expressing the NF-kappaB activator mutant IKK2. **E-F,** Expression of *CXCR4* mRNA (E) and protein (F) in 786-O cells expressing the NF-kappaB activator mutant IKK2. Mean of three experiments (E) and a representative experiment of three (F). Error bars S.E.M.

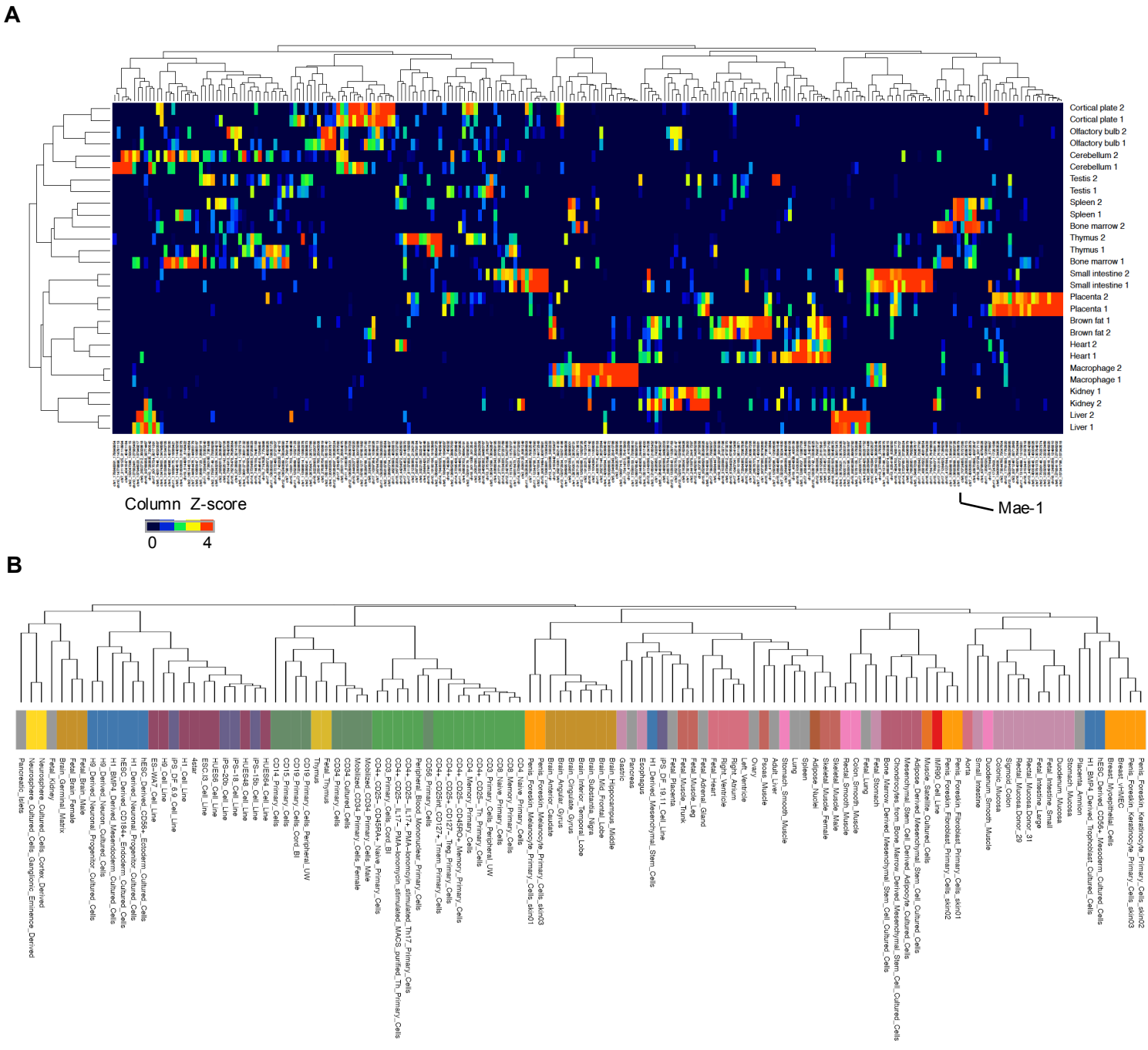

Supplementary Figure 15. MAE overlap with physiological enhancer modules. A, Heatmap showing H3K27ac ChIP-seq signal at 242 orthologous MAE regions in different normal mouse tissues. **B,** Dendrogram showing the normal epigenetic enhancer states associated with the heatmap shown in Figure 7B.

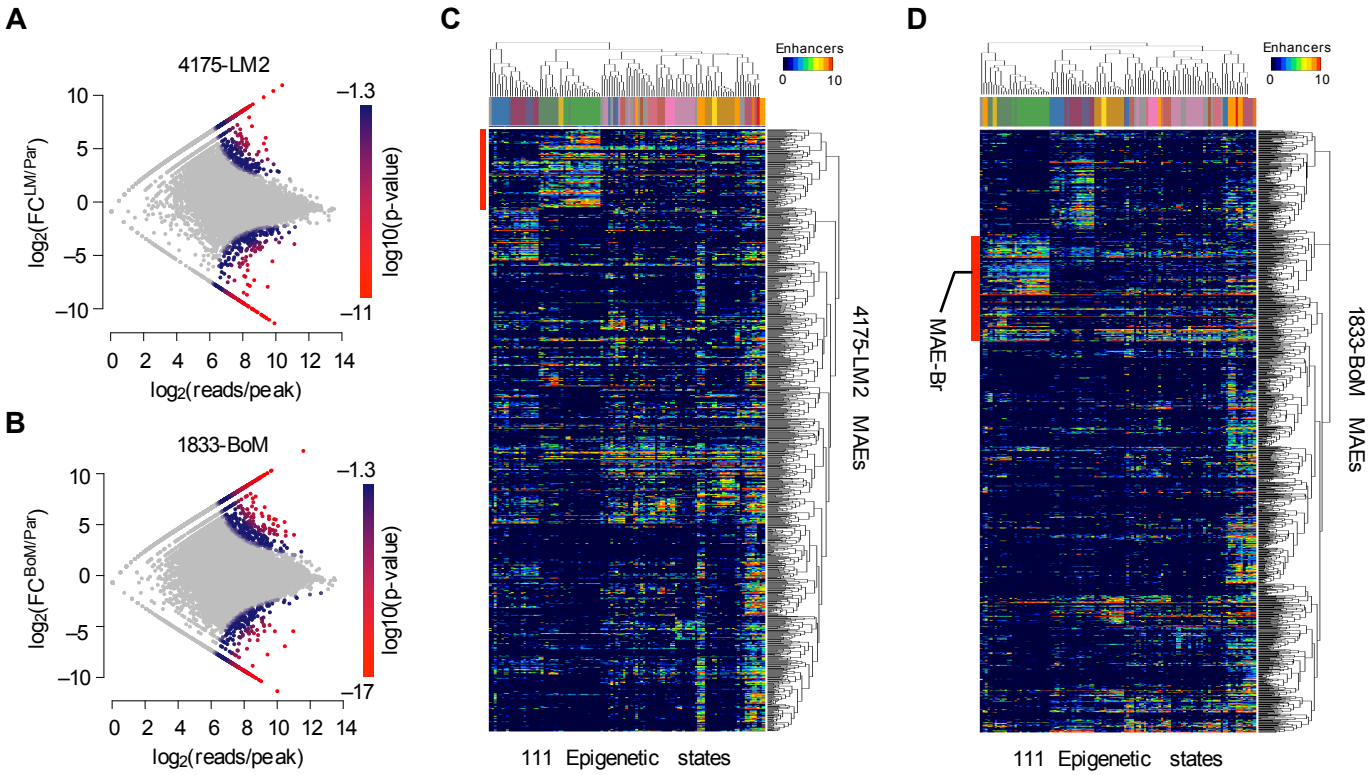

Supplementary Figure 16. MAE activation in metastatic breast cancer cell lines. A-B, ChIP-seq data analysis identifying H3K27ac-enriched and H3K27ac-depleted genomic regions in the lung and bone metastatic variants 4175-LM2 and 1833-BoM when compared to the parental MDA-231 population. **C-D,** Heatmap showing the activity of H3K27ac-enriched lung (C) and bone (D) metastatic enhancers in the 111 physiological tissues from the Roadmap Epigenomics project. Column color code indicates normal tissue type as in Supplementary Figure 15B. Red bar highlights an enhancer module active in various lymphoid tissues.